Proceedings of the ASME 2018 International Design Engineering Technical Conferences and Computers and Information in Engineering Conference
IDETC/CIE 2018
August 26-29, 2018, Quebec City, Quebec, Canada

DETC2018-86391

APPROXIMATE FUNCTIONALLY GRADED MATERIALS FOR MULTI-MATERIAL ADDITIVE MANUFACTURING

Yuen-Shan Leung
Epstein Department of Industrial and Systems Engineering
University of Southern California
Los Angeles, CA

Huachao Mao
Epstein Department of Industrial and Systems Engineering
University of Southern California
Los Angeles, CA

Yong Chen*
Epstein Department of Industrial and Systems Engineering
University of Southern California
Los Angeles, CA

ABSTRACT

Functionally graded materials (FGM) possess superior properties of multiple materials due to the continuous transitions of these materials. Recent progresses in multi-material additive manufacturing (AM) processes enable the creation of arbitrary material composition, which significantly enlarges the manufacturing capability of FGMs. At the same time, the fabrication capability also introduces new challenges for the design of FGMs. A critical issue is to create the continuous material distribution under the fabrication constraints of multi-material AM processes. Using voxels to approximate gradient material distribution could be one plausible way for additive manufacturing. However, current FGM design methods are non-additive-manufacturing-oriented and unpredictable. For instance, some designs require a vast number of materials to achieve continuous transitions; however, the material choices that are available in a multi-material AM machine are rather limited. Other designs control the volume fraction of two materials to achieve gradual transition; however, such transition cannot be functionally guaranteed. To address these issues, we present a design and fabrication framework for FGMs that can efficiently and effectively generate printable and predictable FGM structures. We adopt a data-driven approach to approximate the behavior of FGM using two base materials. A digital material library is constructed with different combinations of the base materials, and their mechanical properties are extracted by Finite Element Analysis (FEA). The mechanical properties are then used for the conversion process between the FGM and the dual material structure such that similar behavior is guaranteed. An error diffusion algorithm is further developed to minimize the approximation error. Simulation results on four test cases show that our approach is robust and accurate, and the framework can successfully design and fabricate such FGM structures.

1. Introduction

In functionally graded materials (FGM), the elemental composition or structure within a domain varies gradually as a function of position, allowing for the gradual transition from one material to another. Hence desired material properties can be tailored locally. Unlike the sharp interface existing in the conventional composite material where most failure is initiated [1], the smooth gradient interface in FGM enables optimal marriage of different materials (such as metals, ceramics, and polymers); hence broader applications based on FGM can be enabled compared to the use of a single material. Since first introduced in Japan in 1984 [2], functionally graded materials have found their applications in aerospace, automobile, medicine, sport, energy, sensors, optoelectronics, etc. A number of survey papers [3] [4] [5] [6] [7] summarized the progresses of FGM research. One exemplary application is an FGM with ceramic-metal structure. The gas-turbine community applies ceramic coatings, referred as Thermal Barrier Coatings (TBC), to protect metals from high-temperature turbine environment [8]. This ceramic-metal FGM produces a thermal barrier with outside temperature of 2000K and inside temperature of 1000K within 10mm thickness [9]. Another emerging application is identified in orthopedic prostheses. The FGM-based grafts (implants) can be adapted to reproduce the local properties of the original bone, which elongates the grafts' lifespan by minimizing the stress shielding effect and reducing the shear stress between the implant and the surrounding bone tissue [10].

Several fabrication approaches have been proposed to manufacture FGMs. In [11], Naebe and Shirvanimoghaddam reviewed most relatively recent FGM fabrication methods, including gas based, liquid phase, and solid phase methods, which can be used to physically or chemically obtain tailored properties. However, most of them can only control the material gradient within one dimension or two dimensions. For example, the gas-based fabrication is basically a layered method, and within each layer, the material composition is identical. In

comparison, with the development of multi-material additive manufacturing technologies [12] [13] [14], FGM objects with arbitrary three-dimensional material compositions can be fabricated.

The individual-voxel controllability in the additive manufacturing process enables heterogeneous material integration, and thus multi-material AM processes provide tremendous flexibility in the design of FGM. Through the advanced AM technologies, designers can refine and optimize products by exploring both the geometric and material distributions to meet customer's requirements. However, the FGM designs are always coupled with manufacturing limitations [6]. For example, most FGM manufacturing methods have the minimum particulate voxel that can only compose a single material within the voxel. For the additive manufacturing, the minimum particulate voxel is the printing resolution of the AM process for each material. However, most FGMs prefer smooth (ideally continuous) gradient interface to minimize the fracture. Hence, an open challenge is how to design digital material compositions such that they can best approximate the desired continuous functional gradient material distribution. This is also the focus of this paper.

A FGM design framework for multi-material AM processes is proposed to fill the research gap on designing, analyzing and fabricating an FGM object. The framework allows a user to design gradient in a spatial domain that has a one-to-one location associated with the physical location where one material could be deposited in the fabrication process. The design then has to be re-adjusted in order for it to be physically fabricated using limited number of base materials that are available in a multi-material AM machine. However, how to determine where to put these limited base materials to achieve the same function as the desired gradient materials is an NP-hard problem. In our framework, we propose to substitute the continuous gradient distribution with two or more base materials in a discrete manner. When the problem becomes small, we can easily find an approximate replacement with our data-driven approach. The gradient design is first divided into a set of cells and the functional behavior of each cell is being matched to a substitution that has similar performance. The characteristic of a substitution is determined by the spatial pattern of the base materials, such that all the substitutions, when putting together, form a heterogenous library. By finding appropriate substitutions from the library, the gradient design can be approximated and the design is guaranteed to be printable by multi-material AM processes.

The framework also facilitates the finite element analysis of FGMs for AM, having a specific location associated with each material. Through FEA we can know the properties of the FGM, as well as the properties of our approximated solution. The resultant performance with respect to the boundary deformation is used to evaluate the accuracy of our method. Furthermore, studies are presented to demonstrate the effect of different discretization schemes that could improve the approximation accuracy.

Compared to the use of topology optimization (TO) to transform gradient into optimal printable distribution, our method is relatively simple and effective. This is because we avoid the burden of iterations; while the TO methods treat each discretization as one design variable and the computational effort will sharply increase when the domain extent increases. This paper aims to introduce a different strategy to design and analyze FGMs. The rest of the paper is organized as follows. Section 2 briefly reviews the FGM related topics. Our proposed method is presented in Section 3. Several testing results and the corresponding discussions are given in Section 4. Finally, Section 5 concludes the paper with remarks on future work.

2. Related Work

To make the paper self-contained, this section briefly reviews the FGM related topics, including FGM fabrication, design, and analysis.

FGM fabrication

FGMs are often fabricated in the specific spatial distribution of the constituent phases such as metals, ceramics, and polymers under continuing and subtle variation in composition makeup. Since the first successful attempt in fabricating FGM using thermal barrier coating in 1984, numerous approaches have been proposed to manufacture FGMs. In the review paper [11], Naebe reviewed most recent FGM fabrication methods, including gas based (e.g., vapour deposition), liquid phase (e.g., plasma spray) and solid phase methods (e.g., powder metallurgy), which can be used to physically or chemically obtain tailored properties. Another survey paper [15] also presented comprehensive insights on the FGM manufacturing processes.

However, most of these methods can only control the material gradient within one dimension or two dimensions. With multi-material additive manufacturing technologies [12] [13] [14] [16], FGM objects with arbitrary three-dimensional material compositions can now be fabricated. Several AM methods can fabricate FGM components with ceramic, metal, or polymer. Typical AM processes with FGM capability include multiple material systems for selective beam sintering [17], multiple-nozzle deposition [18], multiple-powder deposition [19], multiple-droplet dispensing [20] and multiple-vat mask-image-projection-based stereolithography (MIP-SL) [21]. These multi-material AM processes pave a new path to fabricate FGMs and also raise signifcant challenges and new requirements on FGM design.

FGM design methodology

Biomimetic design is learning from nature, and fortunately, FGM is not new to nature. For example, Bamboo, human bone, and shell are all FGMs. A lot of research efforts show that these biological structures change their geometry to adapt to physical environment [22]. Many FGM designs are inspired by these biological structures, which are optimized to an external stimulus. A recent review paper [23] gives a comprehensive understanding of bio-inspired FGM design.

FGM design also evolves with the advance of FGM manufacturing processes. Initially, FGM is only a one-dimensional design problem, because the fabricated FGMs' material composition mainly varies only along the layered direction. For instance, the design of Thermal Barrier Coating is governed by a power law gradient function [24], which determines the material distribution. Hence parametric design is effective and sufficient in designing FGM problems with one-dimensional variations.

When additive manufacturing is applied to the fabrication of FGMs, the design problems becomes much more challenging due to the number of design variables increasing from several function parameters to a vast number of individual voxels with given material compositions. To meet this need, another well-known FGM design methodology called Topology Optimization (TO) has been intensively studied. Topology optimization is regarded as the process of determining the optimal material composition inside a design domain. Readers can refer to [25] [26] [27] for a comprehensive coverage of the recent developments in topology optimization of multi-material problems. However, a down side of topology optimization is it is computationally expensive. To address the design efficiency and manufacturing limitation, we propose a new design methodology in the paper, exemplar-based design, which approximates the continuous material distribution to digital material compositions.

FGM analysis

A typical FGM represents a particulate composite with a prescribed distribution of volume fractions of constituent phases [6]. The particulate composition determines the FGM's material property. The optimal design of FGM is based on the analysis of material property for each particulate composite. Numerous empirical and theoretical models have been proposed to model the FGMs' material property [6]. With the help of numerical simulation, the Finite Element Analysis (FEA) method is prevailing in recent years [28]. Several commercialized and open-source FEA packages are now available for analyzing FGM properties in multiple disciplines. However, FEA is very time-consuming as well, especially for a large domain with detailed mesh. There is a trend to utilize machine learning algorithms to learn the surrogate material property model based on only a few FEA evaluations [29]. The exemplar-based design method proposed in the paper can avoid the iterative FEA evaluations by reusing the FEA results in the exemplars' material property.

In the present work we address the issue of designing and manufacturing FGMs using multi-material AM processes. We mainly focus on the challenge of converting gradient materials design into a design that can be printed with limited number of materials and limited fabrication resolution that are readily available in an AM process. Since the design problem is NP-hard, we propose an efficient data-driven approach to approximate the solution.

3. Methodology

Voxel representation is chosen to represent three-dimensional (3D) computer-aided design (CAD) model in all stages including gradient design, printable design, numerical analysis, and model fabrication since they all rely on discretized volumetric space to specify materials. Fig 1 illustrates the pipeline of our framework. We first create the functional design on a voxel model. The framework will then convert the continuous material layout into a dual-material layout using our exemplar-based approach. The discrete design is able to undergo similar deformation as the continuous design under given loads and constraints. Finally, the dual-material design defined on voxels can be directly used in simulation analysis and model fabrication.

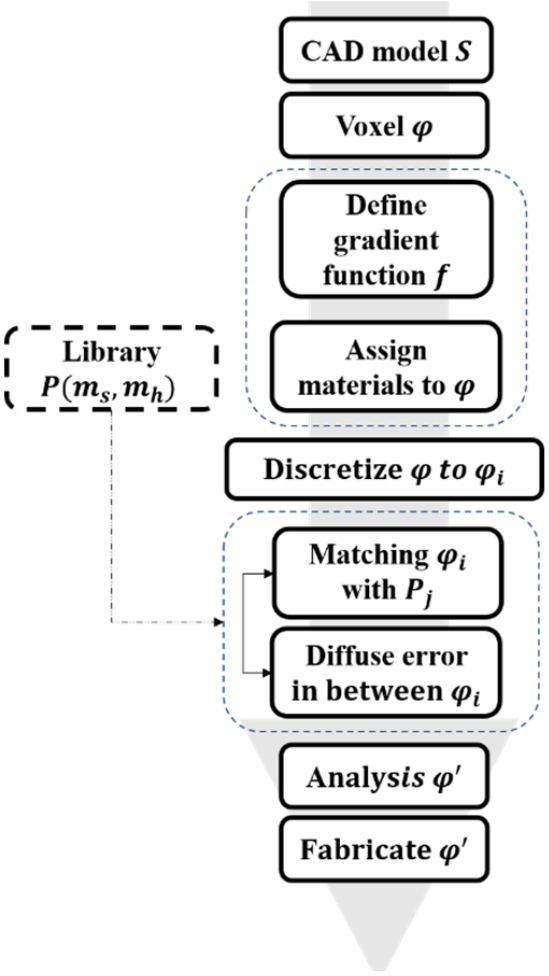

Fig 1: The pipeline of the FGM design framework.

3.1. Voxel-based design with gradient function

A voxel here represents an element where the minimal volume of single material can be deposited in the FGM manufacturing process. Given a CAD model S of an object (2.5D in this paper), we voxelize the S to produce its voxel representation φ and allow each element to associate with one material m, such that a voxel is defined as:

$$\boldsymbol{\varphi_i} = (\boldsymbol{x_i}, \boldsymbol{y_i}, \boldsymbol{z_i}, \boldsymbol{m_i}) \qquad \forall\, \boldsymbol{m_i} \in [\boldsymbol{m_s}, \boldsymbol{m_h}] \qquad (\mathbf{1})$$

where the Young's modulus of the materials must fall within two base materials ($m_s < m_h$).

Initially, a set of candidate elements is selected and set as seed φ_s, where $\varphi_s \subset \varphi$. Then, the rest of the elements will be assigned a material based on a given gradient function f that maps the distance between the centroid of the element and φ_s to the Young's modulus within the range of m_s and m_h. As shown in Fig 2, we present four gradient functions and map every element to single material, such that the rectangle domain exhibits stiffness shift from soft to hard upon the function (color map from blue to red where blue is soft while red is hard). Consider the given function can be non-linear or discontinuous, the resulted FGM can behave in a nonlinear manner, giving much more flexibility in describing composite materials.

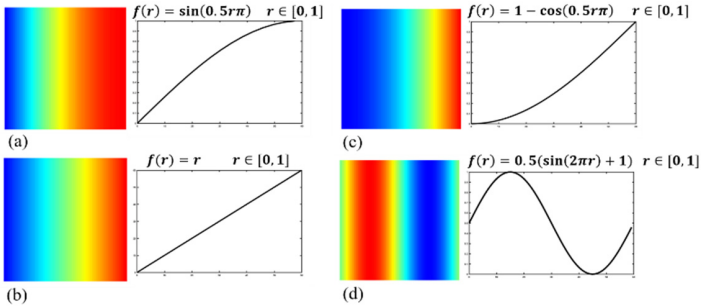

Fig 2: Functionally graded materials in various functions. (a) Sine function; (b) linear function; (c) Cosine function; and (d) Sine function in full cycle.

Although there exist several multi-material AM machines that can directly fabricate FGM objects, the materials that are available in a multi-material AM process are usually limited (e.g. a few types of base materials). To enable AM technology to be used in FGM fabrication, it is desired to approximate design behavior based on two or more base materials such that arbitrary FGM in various functions can be 3D printed even with the material choice constrain.

3.2. Approximate FGM design

Specifically we assume a given FGM design needs to approximate the elastic behavior of the design. The approach to approximate FGM design consists of two steps: (1) matching gradient design with the library patterns in grids, and (2) diffusing localized error to neighbor grids; hence the error can be compensated during the later matching process. In the first step, we propose to discretize the FGM object into *N* small grids and substitute the gradient materials with two base materials individually. The characteristic of each substitution is determined by the spatial distribution of the base materials as a pattern, such that all patterns together form a heterogenous library. By finding the closest behavior-match-pattern from the library, the overall gradient layout can be approximated by two base materials. Such layout can then be 3D printed using two-base-material AM processes.

An important assumption underlying the use of a pattern to replace gradient material change is that spatially distributing of base materials can generate the intermediate mechanical properties of these materials. It has been physically validated by Huang *et al.* [30]. Without loss of generality, our discussion focuses on 2.5D cases for the sake of simplicity, and a similar process can be extended to 3D cases in future.

Given a voxel model φ we discretize the domain into small grids where each of the grids consists of $n \times n$ voxels. We denote each grid as θ and assume $n = 3$ in the following illustration. The matching of materials in a local region by "average" properties (e.g., Young's modulus) has been applied in computer graphics [31] and model fabrication [32]. However, it is not accurate enough when the materials differ vastly in the structure. This is because Young's modulus does not follow a linear relationship with the material composition. Hence matching with average properties may lead to significant error when the difference between two or more base materials is large. Therefore, we define a tensor T^θ to describe the mechanical property of a grid. The tensor contains the longitudinal and transverse deformations incurred by normal stresses σ and shear stresses τ, and it is used for similarity measurement instead of comparing the material composition. In other words, the proposed algorithm uses explicit behavior matching to approximate the target mechanical properties. The tensor is first defined as follows before a library is introduced.

3.2.1. Tensor Definition

Given a square $\mathbf{3 \times 3}$ grid. It has $\mathbf{4 \times 4}$ nodes and is made of *m* linear elastic materials ($m = 3$). The tensor $\boldsymbol{T^\theta}$ is defined by four independent components: $\boldsymbol{e_{xx}}, \boldsymbol{e_{yy}}, \boldsymbol{e_{xy}}$ and $\boldsymbol{e_{yx}}$. The $\boldsymbol{e_{xx}}$ and $\boldsymbol{e_{yy}}$ represent the deformations subjected to axial tensile forces, while the $\boldsymbol{e_{xy}}$ and $\boldsymbol{e_{yx}}$ represent the deformations subjected to axial shear forces as illustrated in Fig 3(b). We assume that Poisson's ratio $\boldsymbol{v}$ is a deterministic constant, and thus only Young's modulus varies in the grid. In response to the applied loads, deformations can be expressed in functions of $\boldsymbol{x}$ and $\boldsymbol{y}$. Considering all the elements in the grid as a whole, the main interest is the explicit behaviors on boundaries. Thus we can concatenate the deformations on exterior nodes to form vectors, which give the tensor as follow:

$$\boldsymbol{T^\theta} = \begin{bmatrix} \boldsymbol{e_{xx}}(\mathbf{3},\mathbf{0}) & \boldsymbol{e_{xx}}(\mathbf{3},\mathbf{1}) & \boldsymbol{e_{xx}}(\mathbf{3},\mathbf{2}) & \boldsymbol{e_{xx}}(\mathbf{3},\mathbf{3}) \\ \boldsymbol{e_{yy}}(\mathbf{0},\mathbf{3}) & \boldsymbol{e_{yy}}(\mathbf{1},\mathbf{3}) & \boldsymbol{e_{yy}}(\mathbf{2},\mathbf{3}) & \boldsymbol{e_{yy}}(\mathbf{3},\mathbf{3}) \\ \boldsymbol{e_{yx}}(\mathbf{3},\mathbf{0}) & \boldsymbol{e_{yx}}(\mathbf{3},\mathbf{1}) & \boldsymbol{e_{yx}}(\mathbf{3},\mathbf{2}) & \boldsymbol{e_{yx}}(\mathbf{3},\mathbf{3}) \\ \boldsymbol{e_{xy}}(\mathbf{0},\mathbf{3}) & \boldsymbol{e_{xy}}(\mathbf{1},\mathbf{3}) & \boldsymbol{e_{xy}}(\mathbf{2},\mathbf{3}) & \boldsymbol{e_{xy}}(\mathbf{3},\mathbf{3}) \end{bmatrix} \qquad (\mathbf{2})$$

where the index (i, j) corresponds to the node index in the grid, and each deformation vector is determined by the nodal displacement. For example, the element $e_{xx}(3,2)$ is derived at node $n(3,2)$ (refer to Fig 3(a)), where the line is subjected to a force acting in the x-direction. The amount of elongation

depends upon the displacement at nodes $n(0,2)$ and $n(3,2)$. If end node displaces $d(3,2)$ and start node displaces $d(0,2)$, the deformation at $e_{xx}(3,2)$ is equal to $d(3,2) - d(0,2)$. Each node along the boundary captures a unique response of the element to the load. Thus, by combining them together, the tensor can form an identification of the grids. Structural finite element analysis can be applied to calculate the nodal displacements and to extract the tensor information.

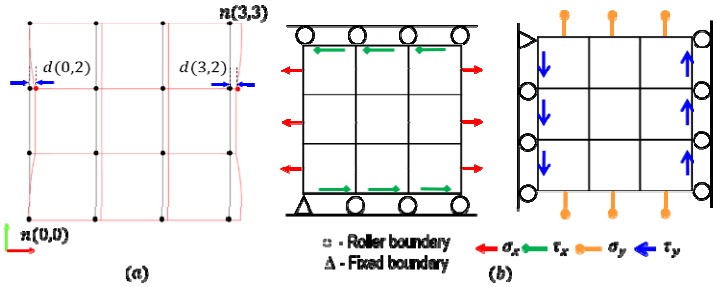

Fig 3: (a) Element $e_{xx}(3,2)$ of deformation vector e_{xx} is derived from two node points. And (b) four boundary conditions (represented in four types of arrow) are applied on a tile to extract the corresponding behavior.

3.2.2. Construct heterogenous library

First of all, as a pre-processing step, we construct a library to enumerate the possible spatially distributed patterns from the base materials. Consider each pattern is defined by a 3-by-3 unit-square grid. Elements in the grid are assigned to one of the base materials such that the combination of these elements in terms of location and the materials in each grid form a unique pattern in the library. The material library is a collection of grid patterns that can have various behaviors when subjected to external forces. The pattern can be constructed in a different size, which could lead to different approximation result. The choice of the pattern size will be discussed in Section 7. Assume two base materials are selected for constructing the library (i.e. $n = 3,\ k = 2,\ e_s\ and\ e_h$), the number of patterns is $k^{N\times N} = 512$. A tensor T^P (P stands for a pattern in the library) is then computed to describe the mechanical properties of each pattern. We employ the k-d tree data structure to store the result and to speed up the high-dimensional search in the matching step.

3.2.3. Similarity Measures for Tensor

To determine the best-match pattern in the library for a grid, we compare its tensor with the library tensors by conducting two similarity calculations. One of the similarity calculations is trend-based, which compares the changes of the current column of a tensor with the last one to see the underlying behavior. Another similarity calculation is to measure the absolute distance between the components of a tensor.

Trend-based Analysis. The purpose of the analysis is to find patterns that have similar behavior, regardless of the actual values. For example, a grid deforms and its boundary remains flat. In this case, we should look for a pattern that generates flat boundary after applying the same loading and constrain.

Now let us consider two tensors, one is from the FGM object (denote as T^θ), and another is from the library (denote as T^P). Then we describe the trend of a tensor as

$$\dot{T^\theta} = \begin{bmatrix} g_{xx}(3,1) & g_{xx}(3,2) & g_{xx}(3,3) \\ g_{yy}(1,3) & g_{yy}(2,3) & g_{yy}(3,3) \\ g_{yx}(3,1) & g_{yx}(3,2) & g_{yx}(3,3) \\ g_{xy}(1,3) & g_{xy}(2,3) & g_{xy}(3,3) \end{bmatrix} \quad (3)$$

where

$$g_x(i,j) = (e_x(i,j) - e_x(i,j-1))/\max\,(e_x(i,j), e_x(i,j-1))$$
$$g_y(i,j) = (e_y(i,j) - e_y(i-1,j))/\max\,(e_y(i,j), e_y(i-1,j))$$

And the similarity of $\dot{T^\theta}$ and $\dot{T^P}$ is defined as the Frobenius norm of their difference:

$$\epsilon_{t-sim} = \|M\| = \left(\sum_{i=1}^{4}\sum_{j=1}^{3}|m_{ij}|^2\right)^{\frac{1}{2}}$$

where

$$M = \dot{T^\theta} - \dot{T^P},$$

and

$$M = \begin{bmatrix} g_{xx}^\theta(3,1) - g_{xx}^P(3,1) & \cdots & g_{xx}^\theta(3,3) - g_{xx}^P(3,3) \\ \vdots & \ddots & \vdots \\ g_{xy}^\theta(3,1) - g_{xy}^P(3,1) & \cdots & g_{xy}^\theta(3,3) - g_{xy}^P(3,3) \end{bmatrix}$$

Distance-based Analysis. Similarly, we define the distance of two tensors, T^θ and T^P, using the same approach:

$$\epsilon_{D-sim} = \|A\| = \left(\sum_{i=1}^{4}\sum_{j=1}^{4}|a_{ij}|^2\right)^{\frac{1}{2}}$$

where

$$A = T^\theta - T^P,$$

and

$$A = \begin{bmatrix} e_{xx}^\theta(3,0) - e_{xx}^P(3,0) & \cdots & e_{xx}^\theta(3,3) - e_{xx}^P(3,3) \\ \vdots & \ddots & \vdots \\ e_{xy}^\theta(0,3) - e_{xy}^P(0,3) & \cdots & e_{xy}^\theta(3,3) - e_{xy}^P(3,3) \end{bmatrix}$$

In this way, we have two lists of patterns that best match the FGM grid, L_{trend} and L_{dist}, with respect to the similarity calculation method. The final step is to determine the closest pattern among them. Therefore, we seek a pattern that has the lowest ranking in both lists, i.e.

$$\arg\min_{x\in P}(L_{trend}(x) + L_{dist}(x))$$

where x is the index for the patterns in the library.

3.2.4. Error Diffusion

Although the matching algorithm gives a good approximation of the gradient input, conversion is not yet fully accomplished. Since an approximation in each grid often leads to an error, the errors of all the grids can be cumulative. Inspired by the error diffusion methods [33] that have been widely used in two-dimensional (2D) color printing, we extend the concept of half-toning in our framework. Errors among neighbors are distributed for error compensation.

We divide the error into four components. Each component represents the deformation error between two grids under the same loadings in single DOF. The error components are spread individually across the domain, and each of them needs to follow the physical governing equation. For example, assuming there are two neighboring grids, c_1 and c_2. They are assigned to materials with Young's modulus E_1 and E_2 respectively. If c_1 is approximated by a Young's modulus $\overline{E_1}$, our target is to find a new value of Young's modulus $\overline{E_2}$ such that the deformation at the end will be the same. Following the stress-deformation equation, the compensation can be governed by

$$\frac{\sigma l}{E_1}+\frac{\sigma l}{E_2}=\frac{\sigma l}{\overline{E_1}}+\frac{\sigma l}{\overline{E_2}}$$

where l is the length of the grid and σ is the stress applied along the x-direction. With this equation, we can understand how c_2 should perform to compensate the approximation error in c_1. We extend this idea to a grid with multiple Young's modulus and the performance is not described simply by a scalar value. The tensor representation is used here to describe both the tensile and shear responses along the x- and y-directions and the complex behavior of the multi-material structure.

Let's define the approximation error for a tile as $\lambda = T_\theta - T_P$ and the components of the error $\lambda = [\Delta x \quad \Delta y \quad \Delta x_\tau \quad \Delta y_\tau]$ are independent of each other. Given an example of diffusing the component Δx_τ into 3 neighbors as shown in Fig. 4. For the first grid at the left bottom corner, error will be diffused to the other three neighbors, and we consider these grids as one block. At first, T^P matches T_1 with the new displacement d_1'. As our goal is to maintain the same length deformation $\Delta l = \bar{l} - l$ of the block after the substitution, we diffuse the error $\Delta d = d_1 - d_1'$ to the grid 2 such that $\Delta l = (d_2 - \Delta d) - d_1'$ remains the same. The new target $d_2' = d_2 - \Delta d$ for grid 2 compensates the error from the grid 1. While for the grid 3 and grid 4, the shear error is diffused such that the top edge of the block can stay in the same position. Every grid in the block will diffuse the error to other three grids and a final diffusing direction (e.g. grid 2 diffuse to grid 1,3,4 could be more accurate than grid 1 to 2,3,4) with minimum error is selected in order to avoid directional bias. After the direction is determined, the three grids that receive error will update their tensors and get ready for diffusion in another block. In other words, we determine the local diffusion for every four grids and repeat the operation over the entire domain in order to improve the overall accuracy.

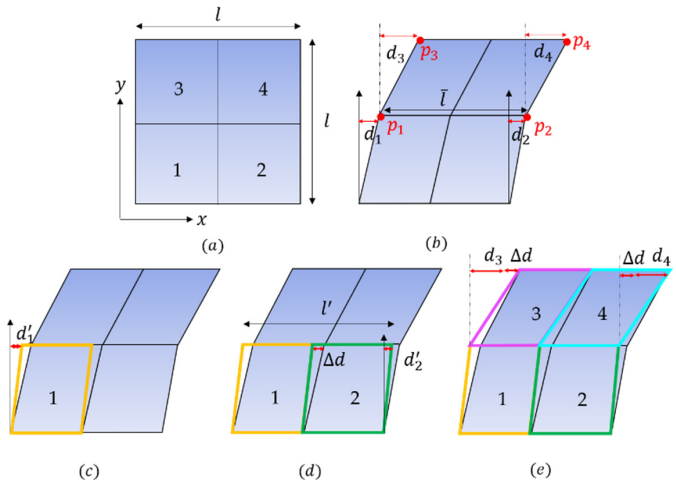

Fig 4: Error diffusion of shear component Δx_τ. (a) A big tile with edge length l is formed by four 3-by-3 grids; (b) the big tile is deformed under shear stress, such that the edge length is deformed to $\bar{l}$; (c) tile T_1' replaces the original tile with new displacement d_1'; (d) in order to compensate the error $\Delta d = d_1 - d_1'$, T_2 has to deform $(d_2 - \Delta d)$ to reach to the same deformed edge length; and (e) for the tiles T_3 and T_4, they have to move Δd to reach to the original positions of top edge.

3.3. Numerical Analysis and Model Fabrication

Once the dual material layout is obtained, we can directly proceed to analysis and fabrication. In this paper, we use finite element analysis to simulate the characteristics of the FGM design and use it to evaluate the behavior of the approximation result.

The deformation behaviors of four gradient designs (Fig 2) on a 2.5D rectangle object in resolution 60×60 are being examined. The rectangle domain is discretized into volumetric elements, and each element is created individually in the FEA software (COMSOL Multiphysics 5.1). The materials are designed on COMSOL 5.1 with Matlab as stated in Section 3.1. We set the Young's modulus of two base materials as $e_s = 2MPa$ and $e_h = 350MPa$, therefore the FGM gradient will be varied within this range. After applying loading and boundary conditions (shown as red arrows in Fig 7), simulation results from COMSOL are obtained and complied.

For physical demonstration, a mask-image-projection based stereolithography (MIP-SL) process [21] is adopted to fabricate heterogeneous objects with digitally controlled multi-material deposition. Our design framework can also be applied to other AM processes. In the multi-material MIP-SL process, an input 3D model is sliced into 2D layers, which are defined as mask images. The generated mask images are then projected onto photocurable resin to selectively solidify corresponding pixels to build the related layer. Based on the 3D model and the material distribution obtained in the framework, mask images are generated as an input to the MIP-SL process. The resolution

of input domain is defined by the printer's *XY* resolution, such that each element corresponds to a regular grid of pixels. Because the framework assumes using two materials in one designed object, the MIP-SL printer projects two mask images to specify the position of two base materials in each layer. An example is shown in Fig 5(c). Currently, the minimal feature that can be reliably built by our MIP-SL system is around 0.25mm, which can be used to define the voxel size in our design framework.

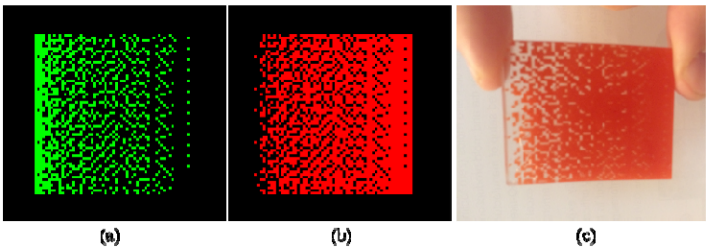

Fig 5: Mask images generated for fabrication. (a) The green pixels indicate the position of hard material; (b) while the red pixels refer to soft material; and (c) the fabrication result.

4. RESULT AND DISCUSSION

The goal of this work is to use two base materials to approximate the mechanical properties of the given gradient material distribution. One of the issues that FGM can address is the displacement and the applied stress can be gradually varied in space, such that specific loading requirements can be met without any abrupt interface at the macroscale. In this paper, we take the deformation as the most important mechanical properties to consider and aim to achieve the same behavior of FGM using only two base materials that a multi-material AM machine provides. To validate our method, we compare the displacements between the approximation result and the given continuous FGM design under the same loading and boundary condition in the FEA simulation.

The distance-based analysis is carried on the boundary nodes to evaluate the accuracy. We compare the deformation of the FGM design and our solution node by node to calculate the maximum error. Fig 6 and Fig 7 compare the behavior of the FGM designs with our approximated dual material designs. We first perform the matching process to convert the continuous design into a dual material layout (Fig 7(b)).

Next, as shown in Fig 7(c), the localized error is compensated using error diffusion. The tensor information is readjusted so that we are able to approximate a better result by coupling the matching process. The result in Fig 7(d) also shows that the errors are further reduced by performing error diffusion twice. These results indicate that the proposed method is capable of converting FGM design to an AM printable layout with predictable deformation behavior. While the approach is heuristic, it enables fast and effective approximation for design problem with very large degrees of freedom.

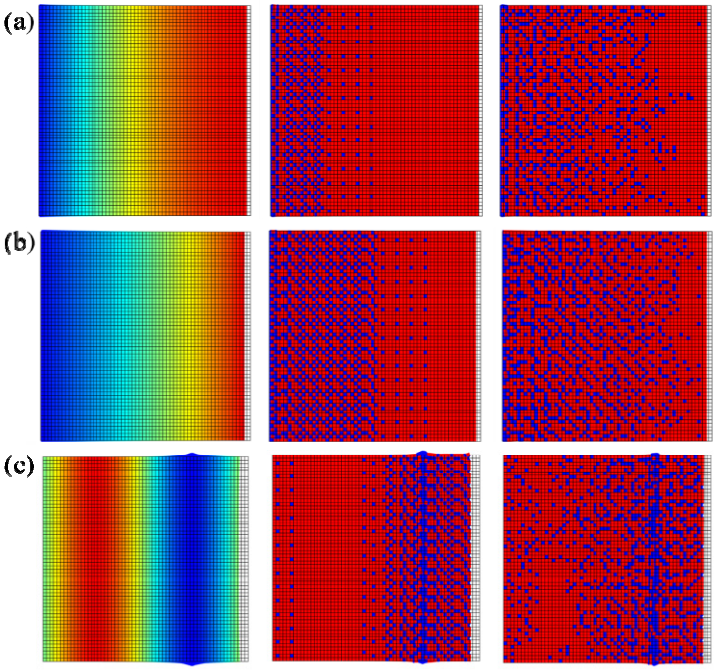

Fig 6: Comparison of deformation between FGM (1^{st}column) and the dual-material layouts generated using method A (2^{nd} column) & B (3^{rd}column). (a) Sine function; (b) Linear function; and (c) Sine-cycle function.

Table 1 presents the approximation errors on the four gradient designs, where the dual material layouts are generated via two methods. The method *A* stands for performing matching using 4×4 library, while the method *B* stands for coupling error diffusion and matching process for approximation. The average and maximum L_2-norm distance, d_{avg} and d_{max}, between their boundary nodes are computed. Generally speaking, adding error diffusion is able to improve the overall performance (refer to Fig 6 for the computed results). However, for the sine-cycle case, the performance of method *A* is better than method *B* (refer to Fig 6(c)). This is mainly because the failure of the error diffusion in approximating the cusp feature.

Table 1: An average d_{avg} and maximum d_{max} L_2-norm distance (% of the voxel length) between a deformed FGM and our approximation results.

Method		Sine	Linear	Cosine	Sin-cycle
A	d_{avg}	0.13%	0.34%	1.12%	0.094%
A	d_{max}	0.38%	0.42%	1.64%	0.84%
B	d_{avg}	0.06%	0.2%	0.6%	0.12%
B	d_{max}	0.24%	0.5%	0.92%	0.985%

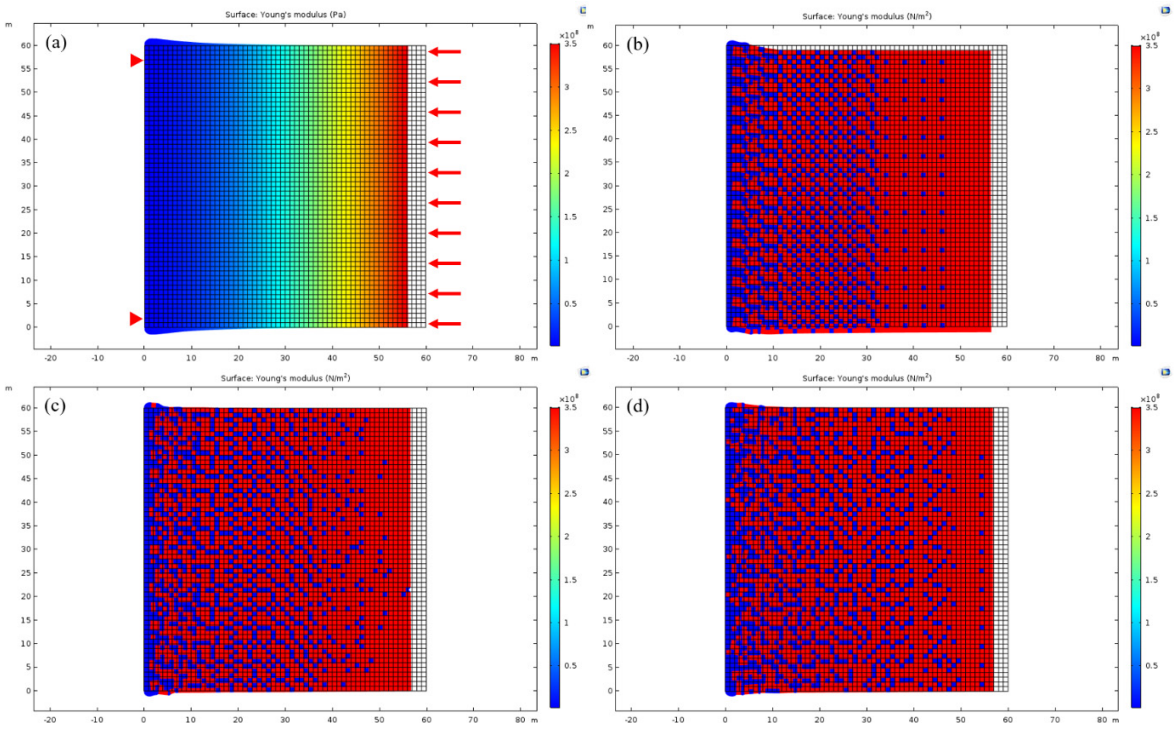

Fig 7: Displacement of the FGM layout and dual-material layout designs. (a) Deformed FGM under prescribed loading and boundary condition. Same loading and boundary condition are applied on the dual-material layout design that created by (b) matching process ($d_{max} = 1.14\%$); (c) error diffusion and matching ($d_{max} = 1.01\%$); and (d) and error diffusion twice and matching ($d_{max} = 0.92\%$).

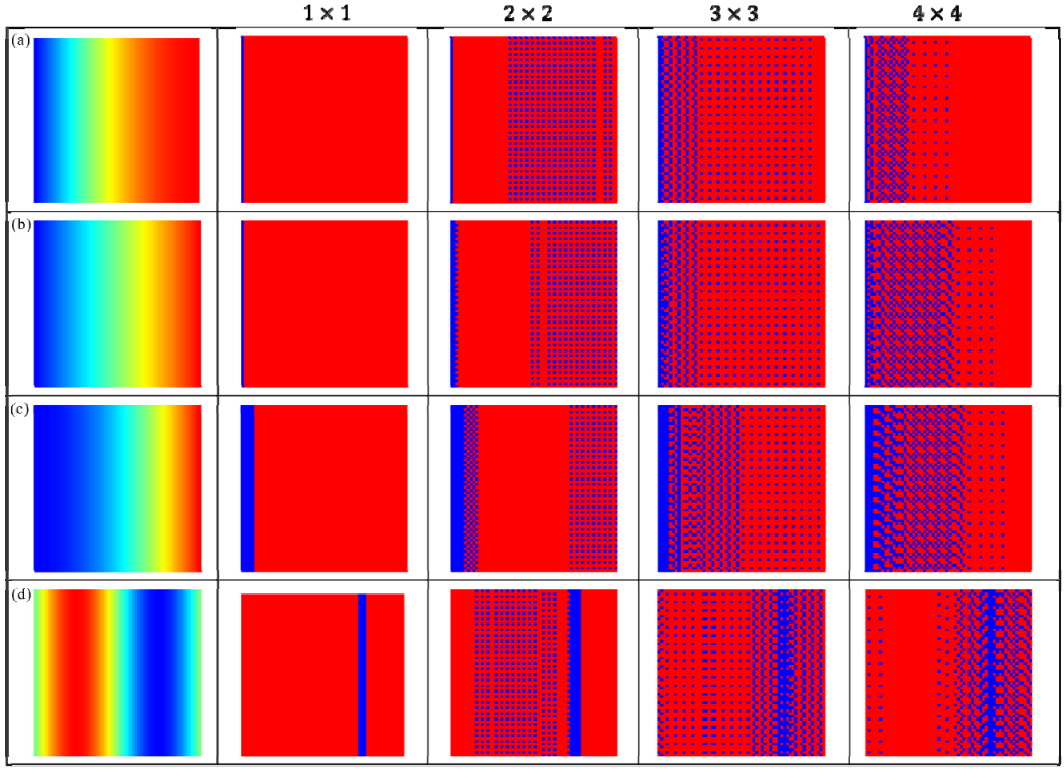

Fig 8: Matching results using different grid size (n) of library. (a) $n = 1$, library size = 2; (b) $n = 2$, library size = 16; (c) $n = 3$, library size = 512; and (d) $n = 4$, library size = 65536.

In addition to error diffusion, another factor that affects the accuracy of approximation is the number of patterns that are used in matching. By increasing the grid size (n), the FGM object is discretized into larger grids; therefore the number of patterns for substitution is increased. Different exemplar set are created depending on the grid size, and the matching performance can be varied. The matching result of using different size of libraries is shown in Fig 8. When the number of patterns is decreasing (i.e. the grid size decreases), the localized error (see Table 2) becomes very large due to the difficulties in finding the closest pattern (i.e. the closest pattern is not close to the gradient grid at all). Therefore, even we readjust the tensor information via error diffusion, a close pattern for substitution can still not be found.

Table 2 presents the matching error induced by the four different set of libraries (see Fig. 8). The result suggests that using the library with grid size $n \geq 3$ is more accurate than $n < 3$. On the other hand, because our method is scalable and able to adapt to different library size, it is possible for us to handle very large domain using larger library size. And there is no limitation on the maximum elements for a pattern. However, it is necessary to consider the computation effort when using larger library size. Therefore, in the future, more focus should be placed on the data processing of very large number of patterns in a library, especially when we extend our framework to 3D cases.

Table 2: Matching error (% of the voxel length) for different library size as shown in Fig. 8.

	1×1	2×2	3×3	4×4
Sin	0.41%	0.37%	0.22%	0.19%
Linear	0.94%	0.611%	0.473%	0.42%
Cos	1.49%	1.17%	1.06%	1.13%
Sin-cycle	1.09%	0.97%	0.68%	0.77%

5. CONCLUSION AND FUTURE WORK

A novel framework to design functionally graded materials (FGM) for advanced manufacturing process such as multi-material additive manufacturing is presented in the paper. FGMs possess all the advantageous material property of different materials by continuously varying the material distribution. However, in order to fabricate FGMs with the multi-material additive manufacturing that has limited number of base materials and fabrication resolution, one way is to build FGMs in a volume discretization manner. Accordingly, a critical issue in the FGM designs for AM is how to generate discretized material compositions that can closely approximate the continuous material distribution. Existing design methods based on topology optimization are time-consuming for the intensive use of finite element analysis simulations, and the designed structures are limited by number of elements used in the simulation. In comparison, the proposed design method is goal-oriented and able to convert gradient material composition into a dual-material composition that can best approximate the mechanical behavior of FGMs. Several numerical simulation results are presented to illustrate our method, and one of the approximation structures was successfully fabricated using the multi-material additive manufacturing technology.

Currently, we have only demonstrated our design methods in 2.5D. The future work would be to explore larger tensor in 3D and to figure out the efficient way of approximating FGM in a more complicated shape. Also, the proposed method could be integrated with topology optimization, which may be able to boost the FEA evaluations required in such a design method.

ACKNOWLEDGMENTS

The work is partially supported by NSF grant (CMMI 1663663). We also acknowledge the help of Wenxuan Jia, an undergraduate student at USC, on the physical fabrication of the test cases.

REFERENCES

[1] S. Wang, "Fracture mechanics for delamination problems in composite materials," *Journal of Composite Materials,* vol. 17, no. 3, pp. 210-223, 1983.

[2] A. Kawasaki and R. Watanabe, "Concept and P/M fabrication of functionally gradient materials," *Ceramics international,* vol. 23, no. 1, pp. 73-83, 1997.

[3] A. Markworth, K. Ramesh and W. Parks, "Modelling studies applied to functionally graded materials," *Journal of Materials Science,* vol. 30, no. 9, pp. 2183-2193, 1995.

[4] A. D. B. Ferreira, P. R. Novoa and A. T. Marques, "Multifunctional material systems: a state-of-the-art review," *Composite Structures,* no. 151, pp. 3-35, 2016.

[5] G. Udupa, S. S. Rao and K. Gangadharan, "Functionally graded composite materials: an overview," no. 5, pp. 1291-1299, 2014.

[6] V. Birman and L. W. Byrd, "Modeling and Analysis of Functionally Graded Materials and Structures," *Applied mechanics reviews,* vol. 60, no. 5, pp. 195-216, 2007.

[7] K. Sairajan, G. Aglietti and K. Mani, "A review of multifunctional structure technology for aerospace applications," *Acta Astronautica,* no. 120, pp. 30-42, 2016.

[8] W. Y. Lee, D. P. Stinton, C. C. Berndt, F. Erdogan, Y.-D. Lee and Z. Mutasim, "Concept of functionally graded materials for advanced thermal barrier coating applications," *Journal of the American Ceramic Society ,* vol. 79, no. 12, pp. 3003-3012, 1996.

[9] M. Niino, T. Hirai and R. Watanabe, "The functionally gradient materials," *J Jap Soc Compos Mat,* vol. 13, pp. 257-264, 1987.

[10] A. Sola, D. Bellucci and V. Cannillo, "Functionally graded materials for orthopedic applications–an update on design and manufacturing," *Biotechnology advances,* vol. 34, no. 5, pp. 504-531, 2016.

[11] M. Naebe and K. Shirvanimoghaddam, "Functionally graded materials: A review of fabrication and properties," *Applied Materials Today,* no. 5, pp. 223-245, 2016.

[12] W. Chiu and K. Yu, "Direct digital manufacturing of three-dimensional functionally graded material objects," *Computer-Aided Design,* vol. 40, no. 12, pp. 1080-1093, 2008.

[13] N. W. Bartlett, M. T. Tolley, J. T. Overvelde, J. C. Weaver, B. Mosadegh, K. Bertoldi, G. M. Whitesides and R. J. Wood, "A 3D-printed, functionally graded soft robot powered by combustion".

[14] J. Wang and L. L. Shaw, "Fabrication of Functionally Graded Materials Via Inkjet Color Printing," *Journal of the American Ceramic Society,* vol. 89, no. 10, pp. 3285-3289, 2006.

[15] R. M. Mahamood, E. T. Akinlabi, M. Shukla and S. Pityana, "Functionally graded material: an overview," in *Proceedings of the World Congress on Engineering 2012*, London, 2012.

[16] B. Zhang, P. Jaiswal, R. Rai and S. Nelaturi, "Additive Manufacturing of Functionally Graded Objects: A Review," in *Proceedings of the ASME 2016 International Design Engineering Technical Conferences and Computers and Information in Engineering Conference*, Charlotte, North Carolina, 2016.

[17] D. L. Bourell, H. L. Marcus, J. W. Barlow, J. J. Beaman and C. R. Deckard, "Multiple material systems for selective beam sintering". U.S. Patent 4,944,817, 31 Jul 1990.

[18] H. Yuna, V. Y. Blouin and M. F. Georges, "Incorporating manufacturability constraints into the design process of heterogeneous objects," *Proceedings of the SPIE,* vol. 5605, pp. 214-225, 2004.

[19] U. Hejmadi and K. McAlea, "Selective Laser Sintering of Metal Molds: The RapidTool Process," in *Solid Freeform Fabrication Symposium*, Texas, August 12th-14th, 1996.

[20] Y. F. Zhu, C. Peng, J. Q. Yang and C. M. Wang, "An Integrated Design and Fabrication Approach for Heterogeneous Objects," *Advanced Materials Research,* Vols. 383-390, pp. 5810-5817, 2012.

[21] C. Zhou, Y. Chen, Z. Yang and K. Behrokh, "Digital material fabrication using mask-image-projection-based stereolithography," *Rapid Prototyping Journal,* vol. 19, no. 3, pp. 153-165, 2013.

[22] Y. Miyamoto, W. Kaysser, B. Rabin, A. Kawasaki and R. G. Ford, Functionally graded materials: design, processing and applications, Boston/Dordrecht/London: Kluwer Academic Publishers, 1999.

[23] U. G. Wegst, H. Bai, E. Saiz, A. P. Tomsia and R. O. Ritchie, "Bioinspired structural materials," *Nature materials,* vol. 14, no. 1, p. 23, 2015.

[24] J. Reddy and C. Chin, "Thermomechanical analysis of functionally graded cylinders and plates," *Journal of thermal Stresses,* vol. 21, no. 6, pp. 593-626, 1998.

[25] M. P. Bendsoe and O. Sigmund, Topology Optimization: Theory, Methods and Applications, Berlin: Springer, 2003.

[26] J. D. Deaton and R. V. Grandhi, "A survey of structural and multidisciplinary continuum topology optimization: post 2000," *Structural and Multidisciplinary Optimization,* vol. 49, no. 1, pp. 1-38, 2014.

[27] N. P. van Dijk, K. Maute, M. Langelaar and V. F. Keulen, "Level-set methods for structural topology optimization: a review," *Structural and Multidisciplinary Optimization,* vol. 48, no. 3, pp. 437-472, 2013.

[28] X. Kou and S. Tan, "A systematic approach for integrated computer-aided design and finite element analysis of functionally-graded-material objects," *Materials & design,* vol. 28, no. 10, pp. 2549-2568, 2007.

[29] G. X. Gu, C.-T. Chen and M. J. Buehler, "De novo composite design based on machine learning algorithm," *Extreme Mechanics Letters,* no. 18, pp. 19-28, 2018.

[30] P. Huang, Y. Li, Zeng, Y. Chen and Jun, "A Digital Material Design Framework for 3D-Printed Heterogeneous Objects," in *ASME. International Design Engineering Technical Conferences and Computers and Information in Engineering Conference, Volume 1A: 36th Computers and Information in Engineering Conference*, 2016.

[31] L. Kharevych, P. Mullen, H. Owhadi and M. Desbrun, "Numerical Coarsening of Inhomogeneous Elastic Materials," *ACM Trans. Graph.,* vol. 28, pp. 51:1-51:8, 2009.

[32] C. Schumacher, B. Bickel, J. Rys, S. Marschner, C. Daraio and M. Gross, "Microstructures to control elasticity in 3D printing," *ACM Trans. Graph.,* vol. 34, pp. 136:1-136:13, 2015.

[33] R. W. Floyd and L. Steinberg, "An Adaptive algorithm for spatial grey scale.," *Proceedings of the Society of Information Display,* pp. 17, 75–77, 1976.